The ALMA-PILS survey: detection of CH₃NCO towards the low-mass protostar IRAS 16293−2422 and laboratory constraints on its formation

N. F. W. Ligterink,[1,2]★ A. Coutens,[3]★ V. Kofman,[1] H. S. P. Müller,[4] R. T. Garrod,[5] H. Calcutt,[6] S. F. Wampfler,[7] J. K. Jørgensen,[6]★ H. Linnartz[1] and E. F. van Dishoeck[2,8]

[1]*Sackler Laboratory for Astrophysics, Leiden Observatory, Leiden University, PO Box 9513, NL-2300 RA Leiden, the Netherlands*
[2]*Leiden Observatory, Leiden University, PO Box 9513, NL-2300 RA Leiden, the Netherlands*
[3]*Department of Physics and Astronomy, University College London, Gower St., London WC1E 6BT, UK*
[4]*I. Physikalisches Institut, Universität zu Köln, Zülpicher Str. 77, D-50937 Köln, Germany*
[5]*Departments of Chemistry and Astronomy, University of Virginia, Charlottesville, VA 22904, USA*
[6]*Centre for Star and Planet Formation, Niels Bohr Institute & Natural History Museum of Denmark, University of Copenhagen, Øster Voldgade 5-7, DK-1350 Copenhagen K., Denmark*
[7]*Center for Space and Habitability, University of Bern, Sidlerstrasse 5, CH-3012 Bern, Switzerland*
[8]*Max-Planck-Institut für Extraterrestrische Physik (MPE), Giessenbachstr. 1, D-85748 Garching, Germany*

ABSTRACT

Methyl isocyanate (CH_3NCO) belongs to a select group of interstellar molecules considered to be relevant precursors in the formation of larger organic compounds, including those with peptide bonds. The molecule has only been detected in a couple of high-mass protostars and potentially on comets. A formation route on icy grains has been postulated for this molecule but experimental evidence is lacking. Here we extend the range of environments where methyl isocyanate is found and unambiguously identify CH_3NCO through the detection of 43 unblended transitions in the ALMA Protostellar Interferometric Line Survey (PILS) of the low-mass solar-type protostellar binary IRAS 16293−2422. The molecule is detected towards both components of the binary with a ratio $HNCO/CH_3NCO \sim 4$–12. The isomers CH_3CNO and CH_3OCN are not identified, resulting in upper abundance ratios of $CH_3NCO/CH_3CNO > 100$ and $CH_3NCO/CH_3OCN > 10$. The resulting abundance ratios compare well with those found for related N-containing species towards high-mass protostars. To constrain its formation, a set of cryogenic UHV experiments is performed. VUV irradiation of CH_4:HNCO mixtures at 20 K strongly indicate that methyl isocyanate can be formed in the solid state through CH_3 and (H)NCO recombinations. Combined with gas-grain models that include this reaction, the solid-state route is found to be a plausible scenario to explain the methyl isocyanate abundances found in IRAS 16293−2422.

Key words: astrochemistry – molecular processes – techniques: spectroscopic – ISM: individual objects: IRAS 16293−2422 – ISM: molecules.

1 INTRODUCTION

Complex organic molecules, defined in astrochemistry as molecules that consist of six or more atoms of which at least one is a carbon atom, are widely found in star-forming regions (Herbst & van Dishoeck 2009). A special category of complex molecules is that of the prebiotics, molecules that can be linked via their chemical structures or reactivity to life bearing molecules, such as amino acids and sugars. Methyl isocyanate (CH_3NCO), also known as iso-

cyanomethane, is a molecule that falls in this category because of its structural similarity with a peptide bond (Fig. 1). This type of bond connects amino acids to form proteins and as such is interesting because it connects to chemistry relevant to the formation of the building blocks of life.

The majority of identified complex molecules has mainly been detected towards high-mass hot cores, such as Orion KL and Sgr B2 (e.g. Blake et al. 1987; Nummelin et al. 2000; Belloche et al. 2013, 2014; Tercero et al. 2013; Crockett et al. 2014; Neill et al. 2014), but over the past decades detections towards low-mass, sun-like, protostars such as IRAS 16293−2422 (hereafter IRAS16293) have been regularly reported as well. IRAS16293 (d = 120 pc) is considered as a protostellar template for

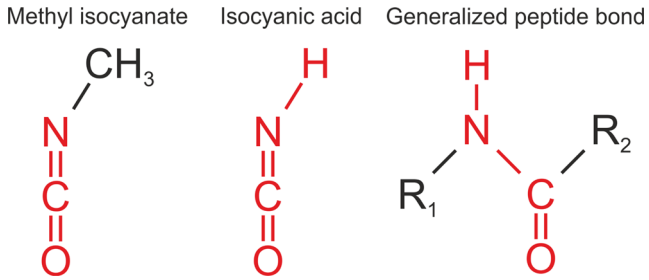Methyl isocyanate   Isocyanic acid   Generalized peptide bond

Figure 1. Structure of methyl isocyanate (left), isocyanic acid (middle) and the generalized structure of a peptide bond (right). In each structure, the components of the peptide bond are highlighted in red. R_1 and R_2 are different molecular functional groups, which can, amongst other possibilities, be a methyl group as for methyl isocyanate.

low-mass sources and is particularly rich in organic molecules (van Dishoeck et al. 1995; Cazaux et al. 2003; Bottinelli et al. 2004; Kuan et al. 2004; Bisschop et al. 2008; Jaber et al. 2014). Jørgensen et al. (2012) demonstrated the capabilities of the Atacama Large Millimeter/submillimeter Array (ALMA) with the detection of the prebiotic molecule glycolaldehyde (see also Jørgensen et al. 2016, for a history of chemical studies of this source). More recently, other complex molecules (acetone, propanal and ethylene oxide) were identified in the framework of the Protostellar Interferometric Line Survey (PILS) (Lykke et al. 2017). Even the deuterated isotopologues of several complex molecules were detected towards this source (Parise et al. 2003; Coutens et al. 2016; Jørgensen et al. 2016).

Unlike other molecules such as isocyanic acid (HNCO) and formamide (NH_2CHO; Bisschop et al. 2007; López-Sepulcre et al. 2015; Coutens et al. 2016), which have a similar peptide-like structure as methyl isocyanate, CH_3NCO only recently started to attract attention in the astrochemistry community. This activity was inspired by a report from Goesmann et al. (2015) that CH_3NCO may be abundantly present on the surface of comet 67P/Churyumov-Gerasimenko, as measured with the Cometary Sampler and Composition (COSAC) instrument of Rosetta's Philae lander. Its measured high abundance of 1.3 per cent with respect to H_2O and CH_3NCO/HNCO = 4.3 was based on the assumption that the mass peak recorded at $m/z = 57$ is dominated by CH_3NCO, as COSAC's low-mass resolution does not allow discrimination of different species with nearly identical mass. Recent measurements with the Rosetta Orbiter Spectrometer for Ion and Neutral Analysis (ROSINA) at much higher mass resolution showed that the CH_3NCO coma abundance is significantly lower (K. Altwegg, private communication). Nevertheless, the possibility of linking complex molecules in star- and planet-forming regions with those present in comets triggered the search for methyl isocyanate in the interstellar medium.

Interstellar CH_3NCO was first detected towards Sgr B2(N) by Halfen, Ilyushin & Ziurys (2015) at low rotational temperatures of $\sim$25 K with a column density ratio of N(HNCO)/N(CH_3NCO) = 35–53 depending on the specific velocity component. Cernicharo et al. (2016) detected methyl isocyanate towards Orion KL at N(HNCO)/N(CH_3NCO) $\simeq$ 15 and T_{ex} = 150 K. Their observations towards the cold pre-stellar core B1-b did not yield a detection of the molecule down to an upper column density limit of $<2 \times 10^{11}$ cm^{-2} or N(HNCO)/N(CH_3NCO) $>$ 42 (based on an HNCO detection towards the same source by López-Sepulcre et al. 2015). In the same paper, publicly accessible Sgr B2 observations from Belloche et al. (2013) were re-analysed with an updated spectral line list and, interestingly, yielded a detection of warm methyl isocyanate at

$T_{ex} \simeq 200$ K and N(HNCO)/N(CH_3NCO) $\simeq$ 40. Attempts to also identify the methyl isocyanate isomer CH_3CNO were unsuccessful down to N(CH_3NCO)/N(CH_3CNO) $>$100.

The astrochemical origin of methyl isocyanate is not yet understood and this is partly due to the limited number of laboratory studies that have been performed. Henderson & Gudipati (2015) tentatively assigned a mass fragmentation peak to CH_3NCO after Vacuum UV (VUV) irradiating solid-state mixtures of NH_3:CH_3OH. In other experiments by Ruzi & Anderson (2012) UV irradiation of frozen *n*-methylformamide (CH_3NHCHO) also yielded methyl isocyanate, although it was concluded to represent a minor product channel.

A number of formation routes have been hypothesized by astrochemists. Halfen et al. (2015) postulated gas-phase formation by HNCO or HOCN methylation:

$$HNCO/HOCN(g) + CH_3(g) \rightarrow CH_3NCO(g) + H(g) \tag{1}$$
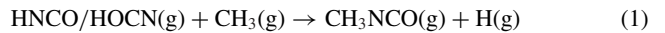
or reactions of HNCO or HOCN with protonated methane, followed by electron recombination:

$$HNCO/HOCN(g) + CH_5^+(g) \rightarrow CH_3NCOH^+(g) + H_2(g) \tag{2}$$

$$CH_3NCOH^+(g) + e^- \rightarrow CH_3NCO(g) + H(g) \tag{3}$$
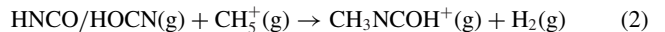
Cernicharo et al. (2016) favoured solid-state formation mechanisms based on the detection of CH_3NCO towards hot cores and its non-detection in the cold-dark cloud B1-b. Particularly, the methylation of HNCO has been mentioned as a possible route to form methyl isocyanate in the solid state, i.e. on the surface of an icy dust grain:

$$HNCO(s) + CH_3(s) \rightarrow CH_3NCO(s) + H(s) \tag{4}$$
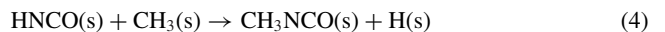
Belloche et al. (2017) used the grain-surface radical-addition reaction $CH_3 + NCO \rightarrow CH_3NCO$ in their models, with most of the NCO formed via H-abstraction of HNCO:

$$HNCO(s) + H(s) \rightarrow NCO(s) + H_2(g) \tag{5}$$

$$NCO(s) + CH_3(g, s) \rightarrow CH_3NCO(s) \tag{6}$$
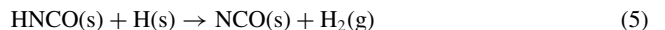
These postulated routes require the reactants to be present in sufficient amounts. Gaseous HNCO is detected in high abundances in protostellar environments and has been imaged in IRAS16293, showing it to be prominent in both sources A and B (Bisschop et al. 2008; Coutens et al. 2016). It likely results from sublimation of OCN^-, known to be a major ice component in low-mass protostellar envelopes (van Broekhuizen et al. 2005). A significant abundance of CH_3 gas is a more speculative assumption since the molecule can only be observed by infrared spectroscopy and has so far only been seen in diffuse gas towards the Galactic Center (Feuchtgruber et al. 2000). Alternatively, CH_3 radicals can be produced *in situ* in ices by photodissociation of known abundant ice components like CH_4 or CH_3OH and then react with HNCO or OCN^-. This is the solid-state route that is investigated here.

In this work, we present the first detection of methyl isocyanate towards both components of the low-mass protobinary IRAS16293 on scales of $<$100 au. An independent detection towards source B is also reported by Martín-Doménech et al. (2017). A set of systematic laboratory experiments is presented in order to validate the solid-state formation routes of CH_3NCO. The observational work is presented in Section 2 and the laboratory work in Section 3. In Section 4, the results of the observations and laboratory experiments are compared and discussed in the context of recent astrochemical models. The conclusions of this paper are given in Section 5.

2 OBSERVATIONS

2.1 The ALMA PILS survey

We searched for methyl isocyanate in the PILS data, an unbiased spectral survey of the low-mass protostellar binary IRAS16293 with ALMA. A full description and data reduction of the survey is presented in Jørgensen et al. (2016). Briefly, this survey covers a spectral range from 329.147 to 362.896 GHz and was obtained with both the 12 m array and the Atacama Compact Array (ACA). The beam size ranges between ∼0.4 and 0.7 arcsec depending on the configuration at the time of the observations. The rms of the combined data sets is about 7–10 mJy beam^{-1} channel^{-1}, i.e. approximately 4–5 mJy beam^{-1} km s^{-1}. To facilitate the analysis, the combined data set used in this paper was produced with a circular restoring beam of 0.5 arcsec at a spectral resolution of 0.2 km s^{-1}.

Two positions are analysed in this study. The first position is offset by one beam diameter (∼0.5 arcsec) from the continuum peak of source B in the south-west direction ($\alpha_{J2000} = 16^h32^m22\overset{s}{.}58$, $\delta_{J2000} = -24°28'32\overset{''}{.}8$) (see high-resolution images in Baryshev et al. 2015). Source B presents narrow lines (FWHM ∼ 1 km s^{-1}). This position is found to be optimal for line identifications, as the lines are particularly bright, do not have strong absorption features towards the bright continuum of source B and do not suffer from high continuum optical depth (Coutens et al. 2016; Jørgensen et al. 2016; Lykke et al. 2017). In this paper, we also analyse source A, which exhibits broader lines than source B making the line identification quite challenging (Pineda et al. 2012). The linewidth varies, however, depending on the spatial separation from this source. With an average FWHM of ∼ 2.5 km s^{-1}, the position $\alpha_{J2000} = 16^h32^m22\overset{s}{.}90$, $\delta_{J2000} = -24°28'36\overset{''}{.}2$ appears to be one of the best positions to search for new species towards source A (0.3 arcsec offset). At this position, the emission is centred at v_{LSR} of ∼0.8 km s^{-1}, blueshifted from the source A velocity of $v_{LSR} = 3.2$ km s^{-1} (Jørgensen et al. 2011).

Bisschop et al. (2008) found HNCO and other nitrogen containing species such as CH₃CN to be more prominent towards source A than source B. Consequently, it is also interesting to check whether there exists a small-scale chemical differentiation amongst the N-bearing species for the two sources.

2.2 Results

Methyl isocyanate is detected towards both components A and B of IRAS16293. The identification is based on spectroscopic data from the Cologne Database for Molecular Spectroscopy (CDMS, Müller et al. 2001, 2005), taken from Cernicharo et al. (2016) as well as from Koput (1986). CH₃NCO is an asymmetric rotor with the NCO group lying at an angle of 140° and a low-lying (∼182 cm^{-1}) C–N–C bending mode v_b. Moreover, the barrier to internal rotation of the CH₃ group is low, only 21 cm^{-1}. The pure rotational spectrum therefore has A and E torsional states and vibrationally excited transitions can become detectable at temperatures of a few hundred K. The labelling of the states used here refers to the quantum numbers J (rotational angular momentum), K_a and K_c (projection of angular momentum on the respective inertial axes) with internal rotation interactions indicated by the quantum number m, with $m = 0$ and ±3 for the A states and $m = 1$, −2 and 4 for the E states (Halfen et al. 2015; Cernicharo et al. 2016).

Using the CASSIS software,[1] we have been able to identify 43 unblended lines of CH₃NCO in the bending ground state ($v_b = 0$) with

upper energy levels E_{up} ranging from 320 to 670 K towards source B (see Table A1). Fig. 3 shows the unblended lines detected towards this component as well as the LTE modelling for two different excitation temperatures at 100 and 300 K. Both excitation temperatures allow us to reproduce the observations; only predicted transitions are observed. Our data are not sensitive to any cold CH₃NCO component since lines with low E_{up} values are missing in the spectral range of the PILS survey. Amongst the complex molecules that were detected and analysed towards source B, some (acetaldehyde and ethylene oxide) exhibit a relatively low excitation temperature of ∼125 K (Lykke et al. 2017), while others (formamide, isocyanic acid, methanol, methyl formate, glycolaldehyde and ethylene glycol) show a higher excitation temperature of ∼300 K (Jørgensen et al. 2012; Coutens et al. 2016; Jørgensen et al. 2016). Their spatial distribution is however rather similar and it is not possible to determine to which category CH3NCO belongs. The methyl isocyanate column density is not very sensitive to the exact value of the excitation temperature: assuming the same source size of 0.5 arcsec as used in the previous PILS studies (Coutens et al. 2016; Jørgensen et al. 2016; Lykke et al. 2017), the CH₃NCO column density is found to be about 3×10^{15} and 4×10^{15} cm^{-2} for $T_{ex} = 300$ and 100 K, respectively. All lines are optically thin. It is expected that for the same assumptions all column densities towards source B are accurate to better than 30 per cent.

Towards source A, most of the lines are blended due to the larger linewidths (∼2.5 km s^{-1}). We can, however, identify 11 unblended lines of CH₃NCO (see Fig. 4). A column density of ∼6×10^{15} and ∼9×10^{15} cm^{-2} (assuming a source size of 0.5 arcsec) is in good agreement with observations for excitation temperatures of 300 and 100 K, respectively, again with an uncertainty of about 30 per cent.

At high excitation temperatures, rotational levels in the first excited bending state ($v_b = 1$) may be populated as well and predictions for possible transitions are shown in Fig. B1. For $T_{ex} = 300$ K, some faint lines can indeed be tentatively attributed to CH₃NCO $v_b = 1$ transitions towards source B. An integrated intensity map of one of the brightest CH₃NCO lines, the $39_{0,39,0}$–$38_{0,38,0}$ transition at 336 339.9 MHz, is presented in Fig. 2. Similarly to other complex molecules, the emission is quite compact with a size of ∼60 au radius and centred near the two sources, with little difference between them (Coutens et al. 2016; Jørgensen et al. 2016; Lykke et al. 2017). For source B, the emission is somewhat offset due to the continuum becoming optically thick on source.

We also searched for spectral evidence of two isomers of methyl isocyanate – acetonitrile oxide (CH₃CNO; Winnewisser et al. 1982) and methyl cyanate (CH₃OCN; Sakaizumi et al. 1990; Kolesniková et al. 2016) – but the corresponding transitions were not found in the PILS data set. From this non-detection, 3σ upper limits of 5×10^{13} and 5×10^{14} cm^{-2} are derived, respectively (assuming an excitation temperature of 100 K). These isomers are consequently less abundant than methyl isocyanate by at least two and one orders of magnitude, in agreement with recent findings towards Orion KL (Cernicharo et al. 2016; Kolesniková et al. 2016).

In view of the important role that HNCO and HOCN may play in the formation of CH₃NCO, we also searched for spectral signatures of these precursor species. The analysis of the PILS data for HNCO towards source B is presented in Coutens et al. (2016). The HNCO lines are optically thick, so lines of the isotopologue HN^{13}CO were analysed and the HNCO column density was derived assuming a ^{12}C/^{13}C ratio of 68 (Milam et al. 2005). To get precise abundance ratios, we re-analysed the HN^{13}CO data using the same data set (with the circular restoring beam of 0.5 arcsec) and obtained
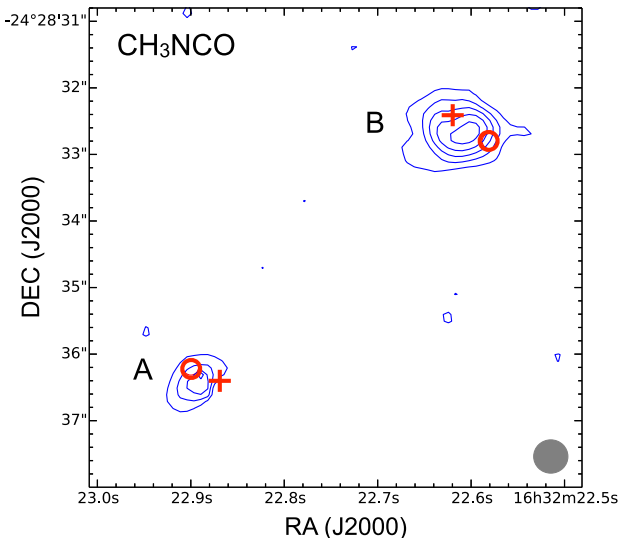
---

[1] CASSIS has been developed by IRAP-UPS/CNRS (http://cassis. irap.omp.eu).

Figure 2. Integrated intensity map of the CH_3NCO $39_{0,39,0}-38_{0,38,0}$ transition at 336 339.9 MHz and $E_{up} = 323.7$ K between 1.7 and 3.7 km s^{-1}. The positions of the continuum of source A (south-east source) and source B (north-west source) are indicated with red crosses, while the positions studied in this paper are indicated with red circles. The contour levels start at 5σ with additional steps of 5σ. The circular restoring beam of 0.5 arcsec size is indicated in grey in the right-hand lower corner.

an HNCO column density of 3.7×10^{16} cm^{-2}, which is within the 30 per cent uncertainty range. The resulting HNCO/CH_3NCO abundance ratio is about 12 towards source B with an uncertainty of less than a factor of 2. Within the error margins, this is similar to the value derived in Orion KL (Cernicharo et al. 2016) or Sgr B2(N2) (Belloche et al. 2016, 2017). For source A, the column density of HNCO is estimated to be about 3.4×10^{16} cm^{-2} ($T_{ex} = 100$ K). The corresponding HNCO/CH_3NCO ratio is consequently about 4 towards this component, with a somewhat larger uncertainty of a factor of 3 due to the difficulty of deriving a precise column density for HNCO because of line blending. Overall, we can conclude that the two HNCO/CH_3NCO ratios are comparable towards the two components of the binary.

Whereas HNCO is readily identified, this is not the case for HOCN. No HOCN lines were detected and a 3σ upper limit of 3×10^{13} cm^{-2} is derived towards source B. HOCN is consequently less abundant than HNCO and CH_3NCO by at least three and two orders of magnitude, respectively. Therefore, it is highly unlikely that the gas-phase formation pathway involving HOCN, as proposed by Halfen et al. (2015) in equations (1) and (2), contributes significantly to the production of methyl isocyanate in this source.

We have also determined the abundance ratios of CH_3NCO with respect to CH_3OH and CH_3CN for comparison with other sources in which methyl isocyanate has been detected (see Table 1). The column density of CH_3OH was estimated based on $CH_3^{18}OH$ by Jørgensen et al. (in preparation) for the one beam offset position towards source B ($\sim 1 \times 10^{19}$ cm^{-2}) using a $^{16}O/^{18}O$ ratio of 560 (Wilson & Rood 1994). With the same assumptions, we estimate a column density of CH_3OH of $\sim 2 \times 10^{19}$ cm^{-2} in source A. CH_3CN was analysed by Calcutt et al. (in preparation) towards both source A ($\sim 8 \times 10^{16}$ cm^{-2}) and source B ($\sim 3 \times 10^{16}$ cm^{-2}). Similarly to the HNCO/CH_3NCO ratio, the abundance ratio of CH_3CN/CH_3NCO is comparable to the values found in Orion KL (Cernicharo et al. 2016) and lower than towards Sgr B2(N1), but again comparable to Sgr B2(N2) (Belloche et al. 2016, 2017). Methanol is, however, clearly

more abundant than methyl isocyanate towards IRAS16293 than towards Orion KL and Sgr B2.

The HNCO/CH_3NCO and CH_3CN/CH_3NCO abundance ratios derived in IRAS16293 are much larger than the lower limits found in comet 67P (>0.2). A proper comparison awaits the new results derived with the ROSINA instrument (Altwegg et al. in preparation).

3 LABORATORY EXPERIMENTS

Grain-surface formation routes of complex molecules have been investigated experimentally for many years using cryogenic set-ups to mimic specific chemical processes under fully controlled laboratory conditions (see Herbst & van Dishoeck 2009; Linnartz, Ioppolo & Fedoseev 2015, for reviews). In the present work, the formation of methyl isocyanate is investigated by energetically processing solid-state CH_4:HNCO mixtures with vacuum-UV radiation. VUV irradiated methane ice is known to efficiently yield methyl radicals (Bossa et al. 2015), and these radicals are expected to further react through surface diffusion with HNCO to form CH_3NCO, as proposed by Goesmann et al. (2015) and Cernicharo et al. (2016), reaction (4). The Cryogenic Photoproduct Analysis Device 2 (CryoPAD2) in the Sackler Laboratory for Astrophysics is used to perform the measurements to investigate the role of methylation of HNCO in methyl isocyanate formation. A short description of this set-up, experimental procedure and reference data is given below.

Note that in these experiments CH_4 is used as the parent of CH_3 but in interstellar space methyl radicals active in the ice may also originate from CH_3OH dissociation (Öberg et al. 2009) or from direct CH_3 accretion from the gas phase. The main aim of this section is to investigate whether or not the proposed solid-state reaction as shown in reaction (4) can proceed at temperatures typical for dark cloud conditions in the interstellar medium (ISM), i.e. independent of the exact precursor species.

3.1 Set-up and method

CryoPAD2 consists of a central chamber operating under ultrahigh vacuum conditions ($P \simeq 10^{-10}$ mbar), to which various instruments are attached. On the top a cryostat is mounted which cools a gold-coated reflective surface down to 12 K. The temperature of this surface can be controlled through resistive heating and varied between 12 and 300 K, with an absolute temperature accuracy better than 1 K. Pure and mixed gases are prepared separately in a gas-mixing system which is attached to a high-precision leak valve to the main chamber and which doses the gases on to the cooled surface. The deposited ice samples are irradiated with VUV radiation from a Microwave Discharge Hydrogen-flow Lamp (MDHL), which emits radiation peaking at 121 nm and a region between 140 to 160 nm, corresponding to photon energies in the range of 7.5–10.2 eV (Chen et al. 2014; Ligterink et al. 2015). The total lamp flux is $(1.1 \pm 0.1) \times 10^{14}$ photons s^{-1} that is determined using a calibrated NIST diode. CryoPAD2 possesses two diagnostic tools to monitor the VUV-induced processes in the ice. The beam of a Fourier-Transform IR Spectrometer (FTIRS) is directed under grazing incidence on to the gold-coated surface, in order to perform Reflection Absorption IR Spectroscopy (RAIRS). The sample preparation and chemical changes under influence of VUV radiation are monitored by recording vibrational fingerprint spectra of molecules on the surface. To decrease the pertubing role of atmospheric CO_2 and H_2O, the system is purged with filtered dry air. The second instrument is a highly sensitive Quadrupole Mass Spectrometer (QMS), with an ionization element at 70 eV, which is able to
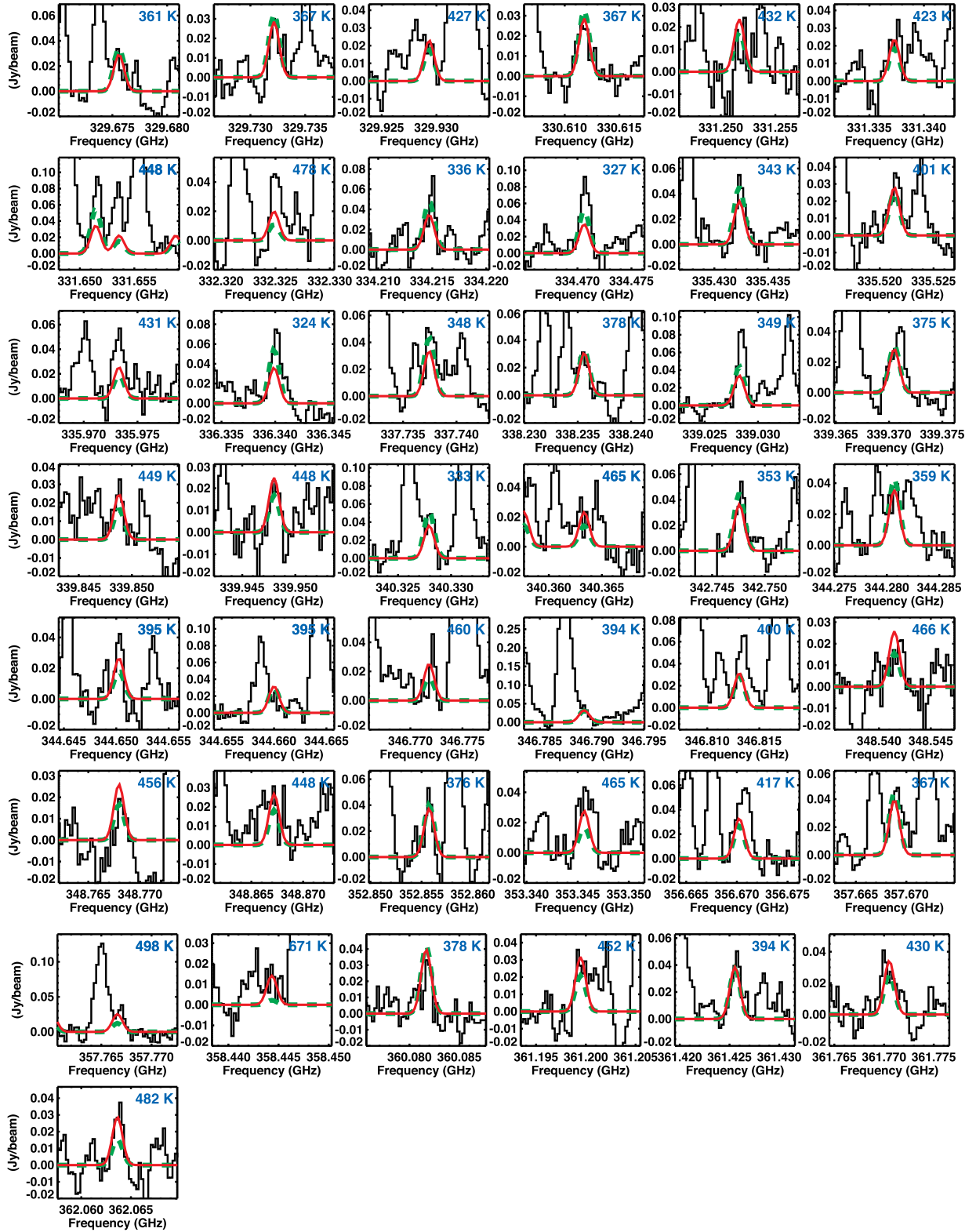
Figure 3. Black: detected unblended lines of CH₃NCO towards source B. Red solid: best-fitting model for $T_{ex} = 300$ K. Green dashed: best-fitting model for $T_{ex} = 100$ K. The E_{up} values of the lines are indicated in blue in the right upper part of each panel.

trace gas-phase molecules in the chamber that are released from the ice surface upon linear heating during a temperature-programmed desorption (TPD) experiment. TPD is a very useful method that allows to identify desorbing species through their specific desorption temperature and mass fragmentation pattern. Unambiguous identifications become possible through the use of isotopologues and searching for the corresponding mass shifts of specific fragments. Obviously, TPD comes with the destruction of the ice.
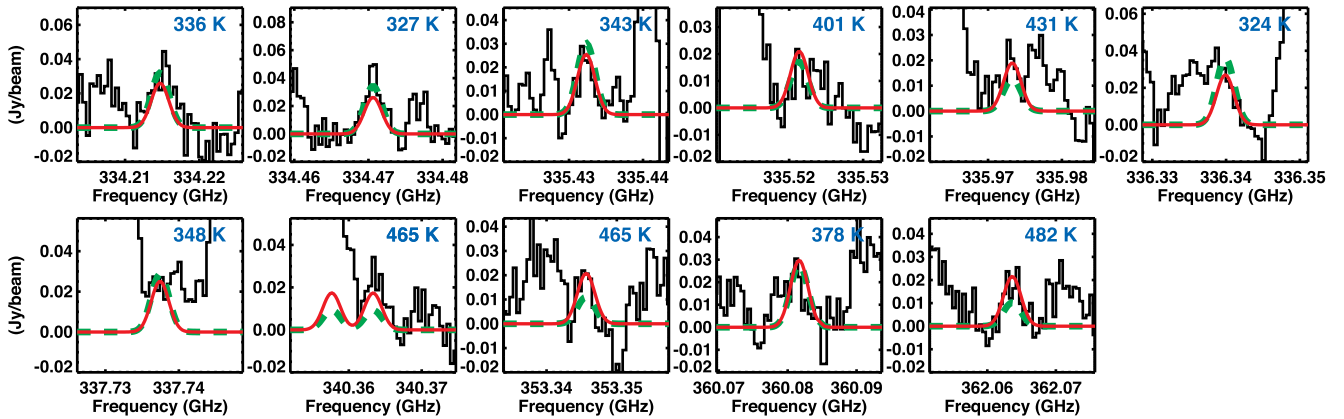
Figure 4. Black: detected unblended lines of CH_3NCO towards source A. Red solid: best-fitting model for $T_{ex} = 300$ K. Green dashed: best-fitting model for $T_{ex} = 100$ K. The E_{up} values of the lines are indicated in blue in the right upper part of each panel.

Table 1. Comparison of molecular abundance ratios towards different sources.

Source	HNCO/CH_3NCO	CH_3CN/CH_3NCO	CH_3OH/CH_3NCO	Reference
IRAS16293 B	12	8	3333	This work
IRAS16293 A	4	9	3200	
Orion KL A	15	10	400	Cernicharo et al. (2016)
Orion KL B	15	25	225	
Sgr B2(N1)	40	50	40	
Sgr B2(N2)	9	10	182	Belloche et al. (2016, 2017)
Comet 67P/C-G	>0.2	>0.2	–	Goesmann et al. (2015) Altwegg et al. (in preparation)

In the experiments CH_4 (Linde Gas, 99.995 per cent purity), $^{13}CH_4$ (Sigma-Aldrich, 99 per cent purity) and HNCO are used. HNCO is produced from cyuranic acid (Sigma-Aldrich, 98 per cent purity), the solid trimer of HNCO, following the protocol described in van Broekhuizen, Keane & Schutte (2004). Impurities of the HNCO production process are removed by freeze–thaw cycles to obtain an HNCO purity of >99 per cent.

For the experiments, samples of pure HNCO and methane and mixtures of $^{13}CH_4$/CH_4:HNCO at 5:1 ratio are prepared. This ratio is within a factor of 2 of that observed for interstellar ices (Öberg et al. 2011) but is particularly chosen to create a large abundance of CH_3 radicals to test whether reaction (4) proceeds or not. Homogeneously mixed ices are grown on the surface at 20 K and irradiated with a total fluence of $\sim 3.3 \times 10^{17}$ photons. During irradiation of the sample, IR spectra are continuously recorded at 1 cm^{-1} resolution. After the irradiation TPD is started, while still recording IR spectra.

The strongest vibrational features of solid methyl isocyanate are found between 2320 and 2280 cm^{-1} (~ 4.34 μm) for the $-N=C=O$ antisymmetric stretching vibration and overtone $2\nu_7$ CH_3 rocking mode. Sullivan et al. (1994) lists these at 2320, 2280, 2270, 2240 and 2228 cm^{-1}, with 2280 cm^{-1} being the strongest band. Zhou & Durig (2009) positioned all bands around 2300 cm^{-1} and Reva, Lapinski & Fausto (2010) put the band for methyl isocyanate in a nitrogen matrix at 2334.7, 2307.9, 2288.9, 2265.2 and 2259.7 cm^{-1}, finding the strongest transition at 2288.9 cm^{-1}. The region around these bands is used to monitor CH_3NCO formation in the ice. We focus on the region between 2400 and 2100 cm^{-1}. From previous experiments it is known that CO_2 (2340 cm^{-1}), OCN$^-$ (2165 cm^{-1}) and CO (2135 cm^{-1}) are produced from HNCO (2265 cm^{-1}) upon irradiation and these photoproducts also have

spectral features in the region characterizing methyl isocyanate (Raunier et al. 2004; van Broekhuizen et al. 2004). Other known products of HNCO irradiation are formamide, urea and formaldehyde, which do not have any interfering IR features in the region of interest. Energetic processing of methane does not yield products that show up in the region of interest. Products that are formed from methane are mainly ethane and to a lesser extent ethene and ethyn (Bennett et al. 2006; Bossa et al. 2015). These species are seen in our spectra at their appropriate frequencies. The abundant formation of ethane demonstrates that CH_3 is indeed produced in the experiments, since ethane is the direct product of methyl-radical recombination.

In order to identify methyl isocyanate in the gas phase using TPD, the mass fragmentation pattern available from the NIST data base[2] is used. The fragmentation pattern at 70 eV comprises unique peaks at $m/z = 57$ and 56 (hereafter also called the primary and secondary mass peaks), which have an m/z 57:56 ratio of 5:2 and these will be used as main TPD mass tracers. Known products of pure HNCO and methane irradiation do not have a mass fragmentation peak at $m/z = 57$ (see also Appendix C).

It is important to mention that methyl isocyanate is severely toxic and specialized laboratories and equipment are needed to work with this substance. This complicates the extensive use of this species and for this reason additional experiments, starting from the pure precursor, have not been performed.
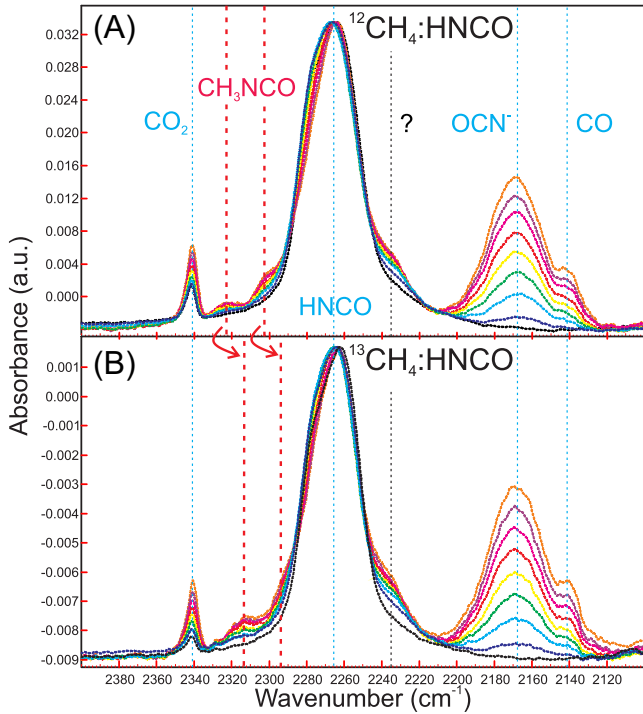
Figure 5. IR spectra taken over time for the $^{12}CH_4$:HNCO (A) and $^{13}CH_4$:HNCO (B) mixture. HNCO and the products CO_2, OCN^- and CO are listed (blue). Spectroscopic features that coincide with CH_3NCO are found at the red lines and show a clear shift with the $^{13}CH_4$ isotopologue. One unidentified peak is found in the right wing of the HNCO peak, indicated by a question mark.

3.2 Results – IR Spectra

Fig. 5 presents the IR spectra recorded during the first 1×10^{17} photons irradiating the $^{12/13}CH_4$:HNCO samples. All spectra are normalized to the HNCO peak. Three known spectroscopic features of CO_2, OCN^- and CO (blue) show up during irradiation. Also, two new features become visible around 2300 cm^{-1} (red), which do not show up while processing samples of pure HNCO or CH_4. Also a clear redshift of about 10 cm^{-1} of the two features is seen between the sample of $^{12}CH_4$ and $^{13}CH_4$, moving transitions at 2322 and 2303 cm^{-1} to 2313 and 2294 cm^{-1}. These spectroscopic features are therefore the result of a product formed in the reaction between methane and isocyanic acid, and, since they are found close to known CH_3NCO features (given by Sullivan et al. 1994; Reva et al. 2010), are plausibly identified with methyl isocyanate. Another feature is seen in the wing of the HNCO peak around 2235 cm^{-1}, which does not clearly shift with methane isotopologues. The origin of this band is unclear.

Bandstrength values for methyl isocyanate are not available from the literature; however, a rough indication of the amount of formed methyl isocyanate versus lost HNCO can be given by making the assumption that the bandstrength of the NCO antisymmetric stretch vibration of methyl isocyanate equals that of the corresponding vibration of HNCO. To obtain the ratio, the integrated area of the 2303 cm^{-1} feature is divided by the integrated loss area of the 2265 cm^{-1} HNCO band for a number of spectra. A ratio of $N(HNCO)/N(CH_3NCO) = 100$–200 is found, which is about an order of magnitude higher than the ratio observed towards IRAS16293. It should be noted that it is not apriori clear whether solid-state laboratory and gas-phase astronomical abundances can
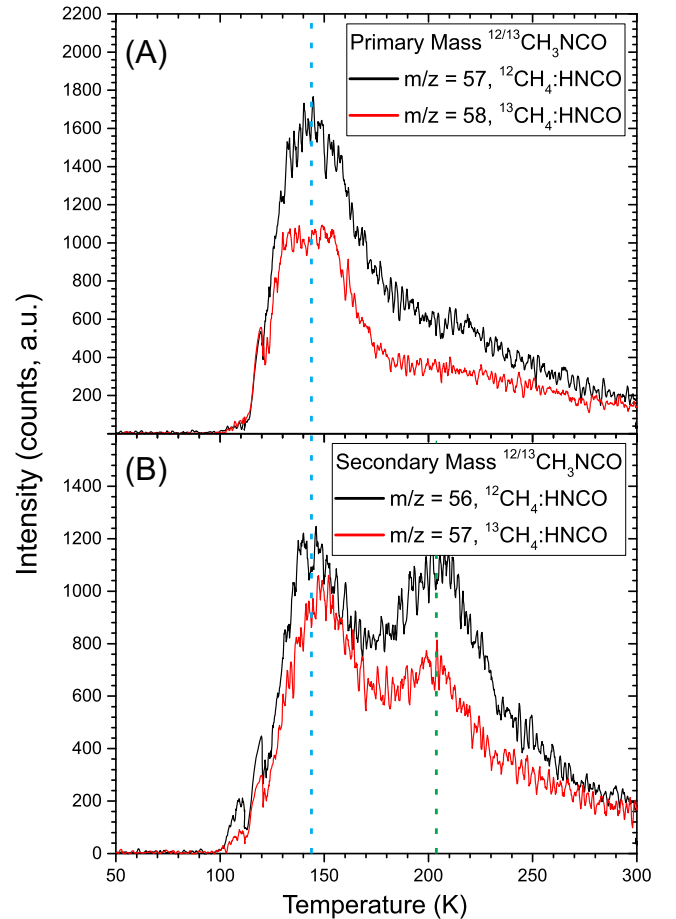

Figure 6. TPD trace of the primary (A) and secondary (B) masses of $^{12/13}CH_3NCO$. Both the primary and secondary masses are seen being released around 145 K (blue line). The secondary mass shows another release peak around 205 K (green), which is suspected to also contribute to first release peak, thus altering respectively the m/z 57/56 and 58/57 ratio.

be directly compared (see e.g. Chuang et al. 2017). It is likely that ongoing gas-phase reactions, for one or the other species, change the solid state to gas-phase ratios. It is also possible that non-linear RAIRS effects can offset the column density (Teolis et al. 2007) or that the CH_3NCO bandstrength is significantly different. In a same manner, CH_3NCO photodestruction may affect the overall abundances.

3.3 Results – temperature-programmed desorption

The desorption temperature of methyl isocyanate has not been reported in the literature, but the TPD traces of our experiments on UV processed CH_4:HNCO ices do show the combined release of the primary and secondary masses of methyl isocyanate $m = 57$ and 56 at 145 K (Fig. 6). The verification experiment of pure HNCO did not show these masses and only $m/z = 56$ (and no 57) was seen after the irradiation of pure methane ice, releasing at 105 K (Fig. C1 in the Appendix). At the 145 K desorption peak the primary over secondary mass ratio is around 1–1.5, lower than the value of 2.5 suggested by NIST upon 70 eV electron impact ionization. The NIST calibration values are a good indicator of the values to be expected, but are to some extent set-up specific. In such cases, the expected reactant can be deposited directly and the fragmentation pattern can be studied and adapted to the set-up in use. This is

unfortunately not possible here due to the aforementioned toxicity of methyl isocyanate. Moreover, contributions from other reaction products cannot be fully excluded. In Fig. 6B a second desorption peak is found around 205 K, which is seen only as a shoulder in panel A. It is unlikely that this peak is associated with methyl isocyanate, instead it shows that the chemical network involves the formation of other species as well. In fact, since the additional product(s) have a mass fragmentation pattern that contributes to the secondary mass of methyl isocyanate, this could explain why the primary/secondary mass ratio does not exactly match with that given by NIST. Additionally, the unidentified product of pure methane irradiation could be trapped in the ice and contribute to other desorption peaks. Therefore, the 145 K desorption peak is still consistent with methyl isocyanate. There is also no other candidate molecule with a primary mass of 57 in the NIST data base that could plausibly explain the TPD spectra.

CryoPAD2 offers the unique feature to combine IR and TPD data, i.e. at the moment a specific ice feature starts thermally desorbing, the IR signal starts decreasing and simultaneously the mass signal starts increasing. In the measurements presented here, this effect is not as clearly visible as in the previous studies (e.g. Öberg et al. 2009), but this may be partly due to the low final S/N of the feature, making it difficult to link RAIRS and TPD signals. The present data are as accurate as possible, but obviously their interpretation would benefit from focused experiments determining the thermal desorption peak of pure CH_3NCO and the IR bandstrengths.

4 LINKING OBSERVATIONS AND LABORATORY DATA

Methyl isocyanate is detected in a significant abundance towards both components of IRAS16293 with an excitation temperature of at least 100 K. The two isomers, CH_3CNO and CH_3OCN, are not detected. Abundance ratios with respect to HNCO and CH_3CN are found to be similar to those found for Orion KL and comparable within a factor of a few to Sgr B2, making a common formation pathway in these three sources likely. Moreover, no chemical differentiation between sources A and B is found. Gas-phase production of CH_3NCO via HOCN (reaction 1) can be seen as insignificant due to the low upper limit on this molecule, but a gas-phase route involving HNCO cannot be excluded.

The laboratory experiments on the formation of CH_3NCO strongly suggest that a solid-state formation scheme is possible, starting from two astronomically relevant precursor species, CH_4 and HNCO. The proposed reaction $CH_3 + HNCO \rightarrow CH_3NCO + H$ indeed seems to proceed, confirming a solid-state reaction pathway, but other routes such as hydrogen stripping $CH_3 + HNCO \rightarrow CH_4 + NCO$ may take place in parallel. Reactions involving the OCN^- anion, which is abundantly formed in these experiments, provide alternative routes. Irradiation of a sample of OCN^-:CH_4, where OCN^- is formed via the acid–base reaction of HNCO with NH_3, will be interesting to study in future work since this anion is also a well-known component of interstellar ice (Boogert, Gerakines & Whittet 2015).

Belloche et al. (2017) have incorporated reactions (5) and (6) (see Section 1) into the large gas-grain model MAGICKAL (Garrod 2013) and simulated the cold collapse + warm-up phase of a hot core region. Although tailored to the high-mass source SgrB2(N), many of the model features are also expected to be valid for the case of IRAS16293. In this model, HNCO is formed by reaction of NH + CO, a route that has been demonstrated experimentally by Fedoseev et al. (2015, 2016). Depending on assumptions about the barriers of the grain-surface reactions involved in the formation of HNCO and CH_3NCO, abundance ratios HNCO/CH_3NCO of 3–50 following ice sublimation are readily found in the models, consistent with the IRAS16293 observations.

5 CONCLUSIONS

The main observational and experimental conclusions are listed below:

(i) Methyl isocyanate is detected for the first time towards a low-mass protostar, IRAS16293, on Solar system scales (emission radius of 60 au). Column densities of $\sim(3–4) \times 10^{15}$ and $\sim(6–9) \times 10^{15}$ cm^{-2} are obtained towards sources B and A, respectively, yielding $N(HNCO)/N(CH_3NCO) = 12$ and 4, with no significant variation between the two sources.

(ii) The abundance ratios of CH_3NCO relative to the N-bearing species HNCO and CH_3CN are similar to those found towards Orion KL and deviate by at most an order of magnitude from Sgr B2.

(iii) The isomers of methyl isocyanate, CH_3CNO and CH_3OCN, are not detected. These species are less abundant than CH_3NCO by at least a factor of 100 and 10, respectively.

(iv) HOCN is not found down to $<3 \times 10^{13}$ cm^{-2}, giving $N(HOCN)/N(HNCO) > 1000$, which makes this an insignificant gas-phase precursor to methyl isocyanate in IRAS16293.

(v) Laboratory experiments strongly suggest that it is possible to form CH_3NCO on an icy surface, irradiating CH_4 and HNCO as astronomically relevant precursor species with VUV light, generating methyl radicals as reactive intermediates to form methyl isocyanate.

The detection of CH_3NCO adds to the growing list of complex molecules known to be present around solar mass protostars, showing that the ingredients for prebiotic molecules are abundant. Future deeper searches for even more complex molecules relevant for the origin of life are warranted.

REFERENCES

Baryshev A. M. et al., 2015, A&A, 577, A129

Belloche A., Müller H. S. P., Menten K. M., Schilke P., Comito C., 2013, A&A, 559, A47

Belloche A., Garrod R. T., Müller H. S. P., Menten K. M., 2014, Science, 345, 1584

Belloche A., Müller H. S. P., Garrod R. T., Menten K. M., 2016, A&A, 587, A91

Belloche A. et al., 2017, A&A, 601, A49

Bennett C. J., Jamieson C. S., Osamura Y., Kaiser R. I., 2006, ApJ, 653, 792

Bisschop S. E., Jørgensen J. K., van Dishoeck E. F., de Wachter E. B. M., 2007, A&A, 465, 913

Bisschop S. E., Jørgensen J. K., Bourke T. L., Bottinelli S., van Dishoeck E. F., 2008, A&A, 488, 959

Blake G. A., Sutton E. C., Masson C. R., Phillips T. G., 1987, ApJ, 315, 621

Boogert A. C. A., Gerakines P. A., Whittet D. C. B., 2015, ARA&A, 53, 541

Bossa J.-B., Paardekooper D. M., Isokoski K., Linnartz H., 2015, Phys. Chem. Chem. Phys., 17, 17346

Bottinelli S. et al., 2004, ApJ, 617, L69

Cazaux S., Tielens A. G. G. M., Ceccarelli C., Castets A., Wakelam V., Caux E., Parise B., Teyssier D., 2003, ApJ, 593, L51

Cernicharo J. et al., 2016, A&A, 587, L4

Chen Y.-J., Chuang K.-J., Muñoz Caro G. M., Nuevo M., Chu C.-C., Yih T.-S., Ip W.-H., Wu C.-Y. R., 2014, ApJ, 781, 15

Chuang K.-J., Fedoseev G., Qasim D., Ioppolo S., van Dishoeck E. F., Linnartz H., 2017, MNRAS, 467, 2552

Coutens A. et al., 2016, A&A, 590, L6

Crockett N. R. et al., 2014, ApJ, 787, 112

Fedoseev G., Ioppolo S., Zhao D., Lamberts T., Linnartz H., 2015, MNRAS, 446, 439

Fedoseev G., Chuang K.-J., van Dishoeck E. F., Ioppolo S., Linnartz H., 2016, MNRAS, 460, 4297

Feuchtgruber H., Helmich F. P., van Dishoeck E. F., Wright C. M., 2000, ApJ, 535, L111

Garrod R. T., 2013, ApJ, 778, 158

Goesmann F. et al., 2015, Science, 349, b0689

Halfen D. T., Ilyushin V. V., Ziurys L. M., 2015, ApJ, 812, L5

Henderson B. L., Gudipati M. S., 2015, ApJ, 800, 66

Herbst E., van Dishoeck E. F., 2009, ARA&A, 47, 427

Jaber A. A., Ceccarelli C., Kahane C., Caux E., 2014, ApJ, 791, 29

Jørgensen J. K., Bourke T. L., Nguyen Luong Q., Takakuwa S., 2011, A&A, 534, A100

Jørgensen J. K., Favre C., Bisschop S. E., Bourke T. L., van Dishoeck E. F., Schmalzl M., 2012, ApJ, 757, L4

Jørgensen J. K. et al., 2016, A&A, 595, A117

Kolesniková L., Alonso J. L., Bermúdez C., Alonso E. R., Tercero B., Cernicharo J., Guillemin J.-C., 2016, A&A, 591, A75

Koput J., 1986, J. Mol. Spectrosc., 115, 131

Kuan Y.-J. et al., 2004, ApJ, 616, L27

Ligterink N. F. W., Paardekooper D. M., Chuang K.-J., Both M. L., Cruz-Diaz G. A., van Helden J. H., Linnartz H., 2015, A&A, 584, A56

Linnartz H., Ioppolo S., Fedoseev G., 2015, Int. Rev. Phys. Chem., 34, 205

López-Sepulcre A. et al., 2015, MNRAS, 449, 2438

Lykke J. M. et al., 2017, A&A, 597, A53

Martín-Doménech R., Rivilla V., Jiménez-Serra I., Quenard D., Testi L., Martín-Pintado J., 2017, preprint (arXiv:1701.04376)

Milam S. N., Savage C., Brewster M. A., Ziurys L. M., Wyckoff S., 2005, ApJ, 634, 1126

Müller H. S. P., Thorwirth S., Roth D. A., Winnewisser G., 2001, A&A, 370, L49

Müller H. S. P., Schlöder F., Stutzki J., Winnewisser G., 2005, J. Mol. Struct., 742, 215

Neill J. L. et al., 2014, ApJ, 789, 8

Nummelin A., Bergman P., Hjalmarson Å., Friberg P., Irvine W. M., Millar T. J., Ohishi M., Saito S., 2000, ApJS, 128, 213

Öberg K. I., Garrod R. T., van Dishoeck E. F., Linnartz H., 2009, A&A, 504, 891

Öberg K. I., Boogert A. C. A., Pontoppidan K. M., van den Broek S., van Dishoeck E. F., Bottinelli S., Blake G. A., Evans N. J., II, 2011, ApJ, 740, 109

Parise B., Simon T., Caux E., Dartois E., Ceccarelli C., Rayner J., Tielens A. G. G. M., 2003, A&A, 410, 897

Pineda J. E. et al., 2012, A&A, 544, L7

Raunier S., Chiavassa T., Duvernay F., Borget F., Aycard J. P., Dartois E., d'Hendecourt L., 2004, A&A, 416, 165

Reva I., Lapinski L., Fausto R., 2010, J. Mol. Struct., 976, 333

Ruzi M., Anderson D., 2012, J. Chem. Phys., 137, 194313

Sakaizumi T., Mure H., Ohashi O., Yamaguchi I., 1990, J. Mol. Spectrosc., 140, 62

Sullivan J., Heusel H., Zunic W., Durig J., 1994, Spectrochim. Acta, 50, 435

Teolis B. D., Loeffler M. J., Raut U., Famá M., Baragiola R. A., 2007, Icarus, 190, 274

Tercero B., Kleiner I., Cernicharo J., Nguyen H. V. L., López A., Muñoz Caro G. M., 2013, ApJ, 770, L13

van Broekhuizen F. A., Keane J. V., Schutte W. A., 2004, A&A, 415, 425

van Broekhuizen F. A., Pontoppidan K. M., Fraser H. J., van Dishoeck E. F., 2005, A&A, 441, 249

van Dishoeck E. F., Blake G. A., Jansen D. J., Groesbeck T. D., 1995, ApJ, 447, 760

Wilson T. L., Rood R., 1994, ARA&A, 32, 191

Winnewisser M., Pearson E. F., Galica J., Winnewisser B. P., 1982, J. Mol. Spectrosc., 91, 255

Zhou S., Durig J., 2009, J. Mol. Struct., 924, 111

APPENDIX A: LINE LIST

Table A1 contains the full list of detected CH_3NCO, $v_b = 0$ transitions towards IRAS16293. A total of 43 lines are observed.

Table A1. Unblended lines of CH_3NCO detected towards source B.

Species	Transition	Frequency (MHz)	E_{up} (K)	A_{ij} (s^{-1})	g_{up}
CH_3NCO, $v_b = 0$	(38 0 0 2 to 37 0 0 2)	329 675.6	361.3	1.71×10^{-3}	77
CH_3NCO, $v_b = 0$	(38 1 0 2 to 37 1 0 2)	329 732.1	367.3	1.71×10^{-3}	77
CH_3NCO, $v_b = 0$	(38 −1 0 −3 to 37 −1 0 −3)	329 929.3	427.1	1.67×10^{-3}	77
CH_3NCO, $v_b = 0$	(38 −1 0 2 to 37 −1 0 2)	330 611.8	367.3	1.71×10^{-3}	77
CH_3NCO, $v_b = 0$	(38 1 0 3 to 37 1 0 3)	331 251.7	431.6	1.74×10^{-3}	77
CH_3NCO, $v_b = 0$	(38 0 0 −3 to 37 0 0 −3)	331 337.3	423.4	1.70×10^{-3}	77
CH_3NCO, $v_b = 0$	(38 2 0 3 to 37 2 0 3)	331 653.6	447.5	1.72×10^{-3}	77
CH_3NCO, $v_b = 0$	(38 3 0 −3 to 37 3 0 −3)	332 324.9	477.7	1.71×10^{-3}	77
CH_3NCO, $v_b = 0$	(39 0 0 1 to 38 0 0 1)	334 214.7	336.5	1.82×10^{-3}	79
CH_3NCO, $v_b = 0$	(39 1 39 0 to 38 1 38 0)	334 470.6	327.3	1.78×10^{-3}	79
CH_3NCO, $v_b = 0$	(39 −1 0 1 to 38 −1 0 1)	335 432.3	342.5	1.83×10^{-3}	79
CH_3NCO, $v_b = 0$	(39 2 0 2 to 38 2 0 2)	335 521.3	401.3	1.83×10^{-3}	79
CH_3NCO, $v_b = 0$	(39 3 0 2 to 38 3 0 2)	335 973.3	431.1	1.82×10^{-3}	79
CH_3NCO, $v_b = 0$	(39 0 39 0 to 38 0 38 0)	336 339.9	323.7	1.82×10^{-3}	79
CH_3NCO, $v_b = 0$	(39 2 38 0 to 38 2 37 0)	337 737.4	348.4	1.83×10^{-3}	79
CH_3NCO, $v_b = 0$	(39 0 0 2 to 38 0 0 2)	338 235.6	377.6	1.85×10^{-3}	79
CH_3NCO, $v_b = 0$	(39 2 37 0 to 38 2 36 0)	339 028.2	349.0	1.85×10^{-3}	79
CH_3NCO, $v_b = 0$	(38 3 0 1 to 37 3 0 1)	339 370.5	374.5	1.75×10^{-3}	77
CH_3NCO, $v_b = 0$	(39 1 0 −3 to 38 1 0 −3)	339 848.8	448.8	1.88×10^{-3}	79
CH_3NCO, $v_b = 0$	(39 1 0 3 to 38 1 0 3)	339 948.0	448.0	1.88×10^{-3}	79
CH_3NCO, $v_b = 0$	(39 1 38 0 to 38 1 37 0)	340 327.9	333.1	1.88×10^{-3}	79
CH_3NCO, $v_b = 0$	(39 2 0 −3 to 38 2 0 −3)	340 363.3	464.6	1.87×10^{-3}	79
CH_3NCO, $v_b = 0$	(40 0 0 1 to 39 0 0 1)	342 747.6	353.1	1.97×10^{-3}	81
CH_3NCO, $v_b = 0$	(40 1 0 1 to 39 1 0 1)	344 280.7	359.2	1.98×10^{-3}	81
CH_3NCO, $v_b = 0$	(40 3 0 2 to 39 3 0 2)	344 650.3	447.7	1.97×10^{-3}	81
CH_3NCO, $v_b = 0$	(40 3 38 0 to 39 3 37 0)	344 660.0	395.0	1.97×10^{-3}	81
CH_3NCO, $v_b = 0$	(40 −1 0 −3 to 39 −1 0 −3)	346 771.8	459.6	1.95×10^{-3}	81
CH_3NCO, $v_b = 0$	(40 0 0 2 to 39 0 0 2)	346 789.2	394.2	1.99×10^{-3}	81
CH_3NCO, $v_b = 0$	(40 1 0 2 to 39 1 0 2)	346 813.1	400.2	1.99×10^{-3}	81
CH_3NCO, $v_b = 0$	(40 1 0 −3 to 39 1 0 −3)	348 541.5	465.6	2.03×10^{-3}	81
CH_3NCO, $v_b = 0$	(40 0 0 −3 to 39 0 0 −3)	348 768.0	456.2	1.99×10^{-3}	81
CH_3NCO, $v_b = 0$	(40 −3 0 2 to 39 -3 0 2)	348 867.2	447.9	1.99×10^{-3}	81
CH_3NCO, $v_b = 0$	(41 1 0 1 to 40 1 0 1)	352 855.7	376.2	2.13×10^{-3}	83
CH_3NCO, $v_b = 0$	(41 3 0 2 to 40 3 0 2)	353 345.6	464.8	2.12×10^{-3}	83
CH_3NCO, $v_b = 0$	(41 −1 0 2 to 40 −1 0 2)	356 670.2	417.3	2.15×10^{-3}	83
CH_3NCO, $v_b = 0$	(41 1 40 0 to 40 1 39 0)	357 668.8	367.0	2.18×10^{-3}	83
CH_3NCO, $v_b = 0$	(41 2 0 −3 to 40 2 0 −3)	357 766.6	498.4	2.17×10^{-3}	83
CH_3NCO, $v_b = 0$	(41 0 0 5 to 40 0 0 5)	358 444.3	671.4	2.16×10^{-3}	83
CH_3NCO, $v_b = 0$	(42 1 42 0 to 41 1 41 0)	360 081.7	378.0	2.23×10^{-3}	85
CH_3NCO, $v_b = 0$	(42 2 0 2 to 41 2 0 2)	361 199.5	452.4	2.28×10^{-3}	85
CH_3NCO, $v_b = 0$	(42 1 0 1 to 41 1 0 1)	361 425.5	393.7	2.29×10^{-3}	85
CH_3NCO, $v_b = 0$	(42 3 40 0 to 41 3 39 0)	361 770.5	429.5	2.28×10^{-3}	85
CH_3NCO, $v_b = 0$	(42 3 0 2 to 41 3 0 2)	362 063.6	482.2	2.28×10^{-3}	85

APPENDIX B: CH$_3$NCO $v_b = 1$

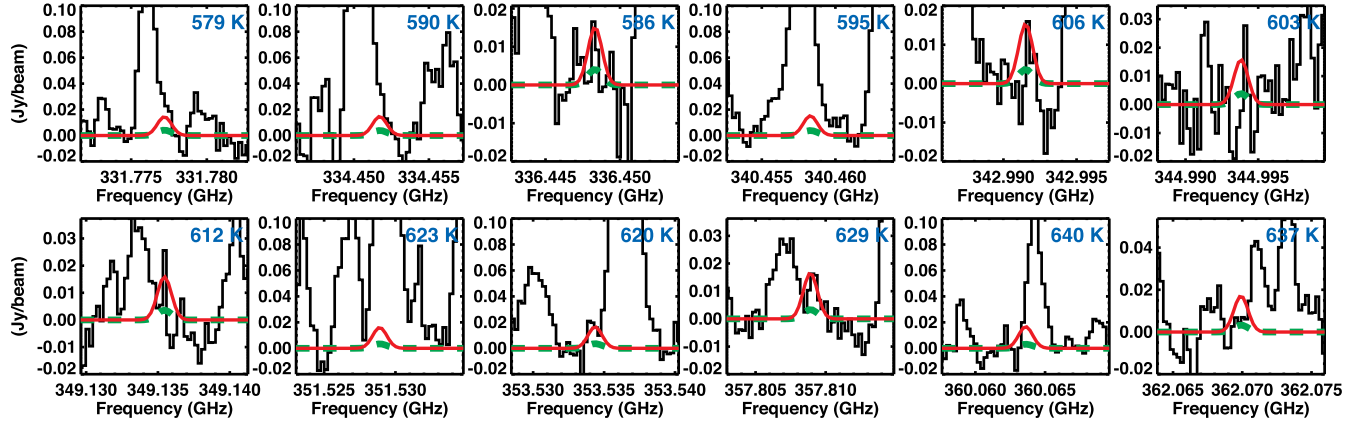Fig. B1 shows the tentative identification of the first excited state of methyl isocyanate.

Figure B1. Predictions for the CH$_3$NCO $v_b = 1$ lines towards source B (red solid: best-fitting model for $T_{ex} = 300$ K; green dashed: best-fitting model for $T_{ex} = 100$ K).

APPENDIX C: $m/z = 56$, 57 AND 58 UPON VUV IRRADIATION OF PURE CH$_4$ AND HNCO SAMPLES

Several publications address the energetic processing of pure HNCO and CH$_4$ ice and much is known about the chemistry that can be induced in these species (Raunier et al. 2004; Bennett et al. 2006; Bossa et al. 2015). Of the known chemical products, none of them contributes to the primary and secondary masses of methyl isocyanate. To verify this, pure methane and isocyanic acid have been VUV irradiated. The HNCO sample (Fig. C1A) does not show any significant release of these masses. However, after irradiation of methane a substantial amount of $m/z = 56$, coinciding with a lesser amount of $m/z = 58$, is seen releasing at a desorption temperature of 105 K. Some m/z 57 is seen to be released as well, although there is no clear peak found in this case. The resulting contribution of $m/z = 56$ can interfere with the $m/z = 57/56$ amu mass ratio of methyl isocyanate.
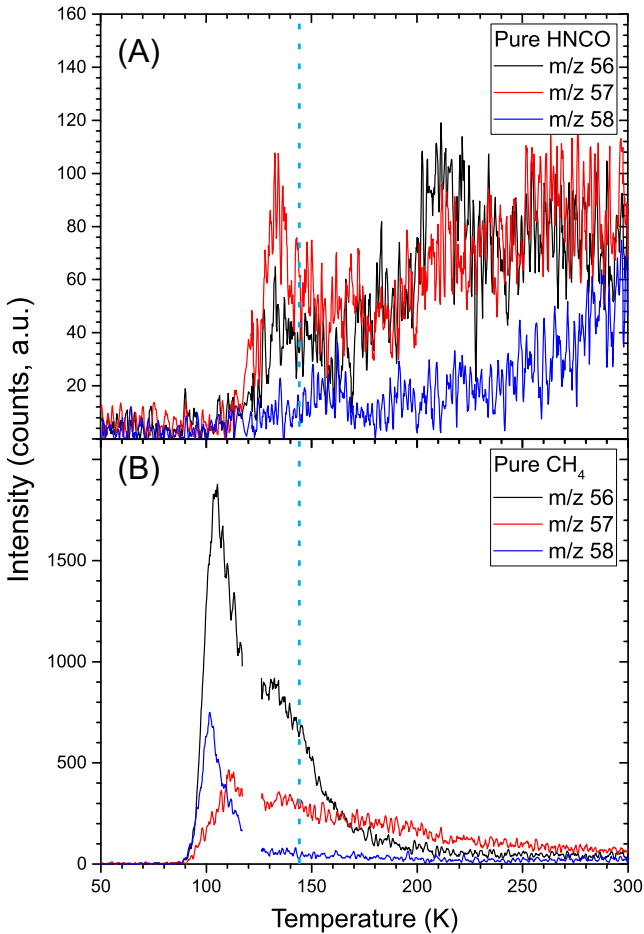
Figure C1. TPD trace of $m/z = 57$ (primary mass CH$_3$NCO), $m/z = 56$ (secondary mass CH$_3$NCO) and $m/z = 58$ after the irradiation of pure HNCO (A) and pure CH$_4$ (B). The desorption peak found in the CH$_4$:HNCO mixtures is indicated by the dashed line at 145 K.

This paper has been typeset from a TeX/LaTeX file prepared by the author.